Molecular BioSystems

PAPER

View Article Online
View Journal | View Issue

Cite this: *Mol. BioSyst.*, 2015, 11, 1410

Slow ligand-induced conformational switch increases the catalytic rate in *Plasmodium falciparum* hypoxanthine guanine xanthine phosphoribosyltransferase†

Sourav Roy,‡[a] Tarak Karmakar,‡[b] Vasudeva S. Prahlada Rao,§[a] Lakshmeesha K. Nagappa,[a] Sundaram Balasubramanian*[b] and Hemalatha Balaram*[a]

Received 13th February 2015,
Accepted 13th March 2015

DOI: 10.1039/c5mb00136f

www.rsc.org/molecularbiosystems

P. falciparum (Pf) hypoxanthine guanine xanthine phosphoribosyltransferase (HGXPRT) exhibits a unique mechanism of activation where the enzyme switches from a low activity (unactivated) to a high activity (activated) state upon pre-incubation with substrate/products. Xanthine phosphoribosylation by unactivated PfHGXPRT exhibits a lag phase, the duration of which reduces with an increase in concentration of the enzyme or substrate, PRPP·Mg^{2+}. Activated PfHGXPRT does not display the lag phase and exhibits a ten-fold drop in the K_m value for PRPP·Mg^{2+}. These observations suggest the involvement of ligand-mediated oligomerization and conformational changes in the process of activation. The dipeptide Leu–Lys in the PPi binding site of human and *T. gondii* HG(X)PRT that facilitates PRPP·Mg^{2+} binding by isomerization from *trans* to *cis* conformation is conserved in PfHGXPRT. Free energy calculations using the well-tempered metadynamics technique show the ligand-free enzyme to be more stable when this dipeptide is in the *trans* conformation than in the *cis* conformation. The high rotational energy barrier observed for the conformational change from experimental and computational studies permits delineation of the activation mechanism.

1 Introduction

Hypoxanthine guanine (xanthine) phosphoribosyltransferase (HG(X)PRT) (E.C. 2.4.2.8) catalyses the Mg^{2+}-dependent reversible transfer of a phosphoribosyl group from 5-phospho-α-D-ribosyl-1-pyrophosphate (PRPP) to the N9 nitrogen atom of 6-oxopurines (hypoxanthine, guanine or xanthine), resulting in the formation of the corresponding mononucleotides, inosine 5′-monophosphate (IMP), guanosine 5′-monophosphate (GMP), or xanthosine 5′-monophosphate (XMP), and inorganic pyrophosphate (PPi). The three-dimensional structures of HG(X)PRT from diverse prokaryotes and eukaryotes are largely

[a] *Molecular Biology and Genetics Unit, Jawaharlal Nehru Centre for Advanced Scientific Research, Jakkur, Bangalore 560064, India. E-mail: hb@jncasr.ac.in; Fax: +91-80-22082877; Tel: +91-80-22082812*

[b] *Chemistry and Physics of Materials Unit, Jawaharlal Nehru Centre for Advanced Scientific Research, Jakkur, Bangalore 560064, India. E-mail: bala@jncasr.ac.in; Fax: +91-80-22082766; Tel: +91-80-22082808*

† Electronic supplementary information (ESI) available: The supporting information contains sections describing the methods and outcomes of construction of W181S and W181S/F197W, purification of PfHGXPRT and mutants (Sections S1 and S2), solvent kinetic isotope effects (Section S3), isothermal titration calorimetry (Section S4) and conformational changes (Section S5) in the dipeptide in the gas phase and in water. A comparison between the *cis* and *trans* apo structure has been included in Section S6. Additionally, data on the hysteretic behavior of PfHGXPRT in potassium phosphate, the oligomeric state of PfHGXPRT in Tris HCl and potassium phosphate buffers, the increase of rate constants with increasing concentration of PfHGXPRT and PRPP, the temperature dependence of lag duration, the relative magnitudes of activation in potassium phosphate and Tris HCl, a comparison of the biochemical properties of PfHGXPRT mutants, the change of fluorescence emission properties of W181S/F197W with an increase in IMP concentration, an estimation of the dissociation constant of the PfHGXPRT·IMP complex using isothermal titration calorimetry and the dependence of the lag duration on PRPP concentration observed using a stopped flow spectrophotometer, the dihedral angle change of the Leu–Lys dipeptide in unbiased MD simulations, gas phase and solvent phase energy barrier calculations, free energy profiles obtained from four different WTM simulations for rotation about the Leu–Lys peptide bond in the ligand-free PfHGXPRT enzyme, the Lys77 side chain interaction with Glu144 and Ile146, the distance between the nitrogen atom (Nξ) of the Lys77 side chain and the carbon atom (Cδ) of the Glu144 side chain *versus* the dipeptide omega dihedral angle (Cα–C–N–Cα), a comparison of Ramachandran plots of free PfHGXPRT and free human HGPRT enzymes, the conformational changes of PfHGXPRT during isomerization of the Leu76–Lys77 peptide bond and the tetramer structure of PfHGXPRT with assignment of the individual subunits are provided. Web enhanced: two web enhanced objects are available in the online version of the paper. This includes two movies in mpeg format that highlight: (1) the opening of loop II, and (2) the conformational change of the Leu76–Lys77 peptide bond. See DOI: 10.1039/c5mb00136f

‡ Both authors have contributed equally to this work.

§ Current address: Novozymes South Asia Pvt. Ltd, Whitefield, Bangalore-560066, India.

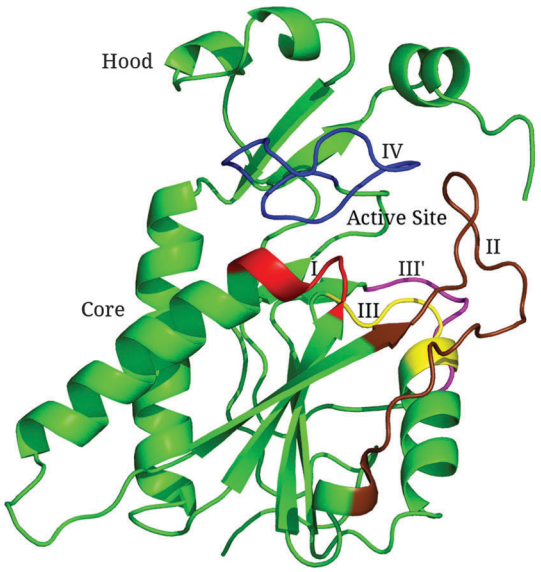

Fig. 1 Structure of PfHGXPRT (1CJB).[5] The hood domain, the core domain and the active site are indicated. The active site loops are loop I (residues 76–81, red), loop II (residues 112–133, chocolate), loop III (residues 146–152, yellow), loop III′ (residues 177–182, magenta) and loop IV (residues 199–214, blue).

similar with the protomer consisting of two domains – the hood and the core – and an active site present in the crevice between the two domains (Fig. 1).[1–7] Examination of the structures of HG(X)PRT shows that the active site is comprised of five loops from a single subunit that are numbered I, II, III, III′ and IV (Fig. 1), the residues of which play important roles in the processes of substrate binding, catalysis and product release.[8–13] The kinetic mechanism of human[14,15] and *Schistosoma mansoni*[16] HGPRTases revealed ordered substrate binding wherein the binding of PRPP precedes the binding of hypoxanthine/guanine. The release of products is also sequential and involves the leaving of PPi prior to IMP/GMP/XMP.[12–16] The processes of substrate binding, catalysis and product release involve a large number of conformational changes in the active site loops, which have been investigated in the cases of *Toxoplasma gondii* HGXPRT[12] and human HGPRT.[13] These changes are largely similar in the two enzymes, with the first event being the isomerization of the Leu78–Lys79 (*T. gondii* numbering) peptide bond (in loop I), which creates a cavity for PRPP binding. This is followed by a sequence of events that involves ordering of loop III, reorientation of Asp150 to function as a catalytic base, binding of the 6-oxopurine through stacking on Trp199 of loop IV, the formation of salt bridges by Arg182 of loop III′ with the side chain carboxyl groups of Asp150 and Asp197 and finally, the closure of loop II, which serves to sequester the unstable reaction intermediates from the bulk solvent. After product formation, the sequential release of PPi followed by the nucleoside monophosphate is facilitated by the weakening of hydrogen bonds and the salt bridge network. All the conformational changes are now reverted, and the enzyme attains its original state for another cycle of catalysis.

HGXPRT in the protozoan parasite *Plasmodium falciparum* is an essential enzyme as it provides the only route for the synthesis of IMP through the salvage of host hypoxanthine. Like the *T. gondii* homolog and unlike the human version, the *P. falciparum* enzyme has an additional specificity for xanthine.[17–21] Although the overall structure of *P. falciparum* HGXPRT (PfHGXPRT) is similar to *T. gondii* HGXPRT and human HGPRT,[2,5,22,23] the enzyme in solution displays kinetic features that are distinct.[24] The crystal structures of human HGPRT, *T. gondii* and *P. falciparum* HGXPRT indicate that the biologically relevant oligomeric state is a tetramer. In solution, the human enzyme is a tetramer while the *P. falciparum* enzyme exhibits an equilibrium between dimer and tetramer, whose populations are modulated by PRPP binding and buffer composition.[25] Earlier studies have shown that PfHGXPRT exhibits weak activity that increases significantly upon pre-incubation with the product IMP.[24] The objective of this study is to characterize the activated (pre-incubated with ligand(s)) and unactivated (without pre-incubation) states of PfHGXPRT and elucidate the mechanism of switching to the activated state. Large energy barrier values obtained from the rate constants of activation suggest the possibility of isomerization of the Leu–Lys peptide bond to mediate the activation process. Molecular dynamics simulations of the ligand-bound and the free enzyme reveal dynamic information about this protein in two different states. The opening of a gate (the distance between Cα of Asn206 in loop IV and Cα of Asn118 in loop II) of the free enzyme was observed during unbiased molecular dynamics simulations. Furthermore, free energy calculations were performed focusing mainly on the dipeptide present at the reaction center. The flipping of the dipeptide from *trans* to *cis* creates space to accommodate the substrate in the active site cavity. The energy barrier for this bond rotation, obtained from free energy calculations, agrees with the experimental value estimated from reaction rates, suggesting the isomerization of the dipeptide as a critical component of enzyme activation.

2 Materials and methods

2.1 Materials

Resins for ion exchange and size-exclusion chromatography were obtained from GE Life Sciences Ltd, Uppsala, Sweden. 6-oxopurines, nucleotides (IMP, GMP, XMP), PRPP, D_2O, Sephadex G-25 and all other chemicals were procured from Sigma Aldrich Inc., USA. *Escherichia coli* strain SΦ609 (*ara*, *Δpro-gpt-lac*, *thi*, *hpt*, *pup*, *purH*, *J*, *strA*), a knockout strain for hypoxanthine phosphoribosyltransferase (HPRT) and xanthine guanine phosphoribosyltransferase (XGPRT), was a kind gift from Dr Per Nygaard, Copenhagen, Denmark.

2.2 Construction of PfHGXPRT mutants F197W and W181S/F197W and purification of enzymes

The mutant F197W was generated by a two-step PCR method that involved megaprimer generation[26] and full-length gene amplification using pTrc99A-PfHGXPRT as the template and 5′CCTGATCAC**TGG**GTGTTGGT3′ as the mutagenic primer. The positive clones were verified by DNA sequencing and checked

for expression after transformation of the pTrc99A-F197W construct into *E. coli* strain SΦ609. The mutants, W181S and W181S/F197W were generated by a quick change PCR method, which is described in Section S1 of the ESI.† The protocol for purification of the enzymes is provided in Section S2 of the ESI.†

2.3 Activity measurements

Phosphoribosylation activity by both unactivated and activated states of PfHGXPRT was monitored at 296 K using Hitachi U-2810 or U-2010 UV-Visible spectrophotometers (Tokyo, Japan). A standard assay mix for unactivated PfHGXPRT consisted of 50 μM hypoxanthine or guanine or 200 μM xanthine, and 3 mM PRPP in 100 mM Tris HCl at pH 7.4, unless otherwise specified. The concentration of free $MgCl_2$ was maintained at 12 mM. A K_d value of 0.59 mM for the PRPP·Mg^{2+} complex[27] was used to calculate the concentration of free $MgCl_2$ at every concentration of PRPP. To achieve the activated state, the enzyme was pre-incubated at a concentration of 30 μM with different ligand(s) in the presence of 5 mM dithiothreitol (DTT). Assay conditions for activated PfHGXPRT were same as those for the unactivated state except for the PRPP concentration, which was maintained at 1 mM. Reactions were initiated with 1 μM enzyme in the case of unactivated PfHGXPRT and 0.2 μM in the case of activated PfHGXPRT. The activated enzyme was directly added to the reaction mixture without prior dilution. A difference in extinction coefficient of 1900 M^{-1} cm^{-1} at 245 nm was used to monitor hypoxanthine phosphoribosylation, 5600 M^{-1} cm^{-1} at 257.5 nm was used for guanine phosphoribosylation and 3794 M^{-1} cm^{-1} at 255 nm was used for xanthine phosphoribosylation.[24,25] Assay protocols were same for the mutants F197W and W181S/F197W.

Xanthine phosphoribosylation was also monitored with unactivated PfHGXPRT using a spectrophotometer attached to a stopped-flow module (SFM-300, Biologic, France). 5 μM unactivated PfHGXPRT was mixed with an assay mix containing 200 μM xanthine, 2 mM PRPP and 26 mM $MgCl_2$ in a 1 : 1 ratio by volume. The total volume of each reaction mix was 126 μl. The total flow rate for mixing was 7 ml s^{-1} with a dead time of 4.3 milliseconds. The duration of the assay was 160 seconds where each data point was acquired every 20 milliseconds, resulting in a total of 8000 data points for the entire trace. The reaction was carried out in both 100 mM Tris HCl and 10 mM potassium phosphate, at pH 7.4 at 296 K. All measurements were performed at least 3–5 times.

2.4 Measurement of rate constants for IMP association and dissociation using PfHGXPRT mutants by stopped-flow fluorescence studies

The mutants F197W and W181S/F197W were used to measure overall rate constants (k_{obs}) for relaxation to equilibrium upon IMP binding, using a spectrofluorimeter attached to a stopped-flow module (SFM 300, Biologic, France). Time courses of change in fluorescence emission were acquired after excitation at 295 nm using a 320 nm cut-off filter. The total duration of each scan was 4 seconds with 500 μseconds for each data point, resulting in a total of 8000 data points. The dead time was fixed at 4.3 milliseconds, and total flow rate was 7 ml s^{-1}. The concentration of F197W was fixed at 5 μM with varied IMP concentrations of 1, 2, 3, 4 and 5 μM. In the case of W181S/F197W, the enzyme concentration was fixed at 3 μM with the varied IMP concentrations being 0.5, 1, 2, 3 and 4 μM. Values of k_{obs} were plotted against IMP concentrations and fitted to the following equation:[28]

$$k_{obs} = k_{on}[L] + k_{off}, \quad \text{(i)}$$

where k_{on} and k_{off} represent the second order and first order rate constants for binding and dissociation, respectively. k_{obs} represents the overall rate constant for relaxation to equilibrium upon binding with IMP. Values of k_{obs} at every IMP concentration were estimated by fitting the time courses of fluorescence emission to eqn (ii), which represents a second order process.

$$Y(t) = at + b + \{c/(1 + k_{obs}t)\} \quad \text{(ii)}$$

In the equation, $Y(t)$ is fluorescence emission (in volts) at any time t, a is the slope of the time course, b represents offset (offset corresponds to the fluorescence emission at equilibrium), c is the amplitude of the fluorescence change (in volts) and t represents time. The dissociation constants (K_d) for the F197W·IMP and W181S/F197W·IMP complexes were estimated from the ratio k_{off}/k_{on} and also by monitoring the steady-state fluorescence emission properties using a Hitachi F-2500 spectrofluorimeter (Tokyo, Japan) at IMP concentrations ranging from 0.5–20 μM, with the concentrations of both mutants fixed at 5 μM. The excitation wavelength was set at 295 nm. Eqn (iii) for one site binding was used to estimate the dissociation constant K_d for the [enzyme·IMP] complexes.

$$\%\ \text{quenching} = \{B_{max} \times [IMP]\}/(K_d + [IMP]), \quad \text{(iii)}$$

where B_{max} represents quenching at the highest concentration of IMP used, [IMP] represents IMP concentration and % quenching was calculated by the relation: $\{(I_{em[IMP]} - I_{em0})/I_{em0}\} \times 100$, where $I_{em[IMP]}$ is the emission intensity of the proteins F197W or W181S/F197W at any particular concentration of IMP and I_{em0} is the emission intensity of the proteins F197W or W181S/F197W in the absence of IMP. Fitting of data to all of the above equations was done using Graph Pad Prism, version 5 (Graph Pad Software Inc., San Diego, California). These experiments were repeated at least twice.

2.5 Estimation of the kinetic parameters of the unactivated and activated states of PfHGXPRT

The kinetic parameters for both unactivated and IMP-activated PfHGXPRT were estimated at varied 6-oxopurine and PRPP concentrations with 100 mM Tris HCl and 10 mM potassium phosphate as the assay buffers containing 12 mM $MgCl_2$, both maintained at pH 7.4.

The experimental details for the estimation of the kinetic parameters in 100 mM Tris HCl at pH 7.4 are as follows. For estimation of the K_m value for PRPP for unactivated PfHGXPRT, the concentration of PRPP was varied from 0.1–3 mM in the case of hypoxanthine phosphoribosylation, 0.1–3.5 mM in the

case of guanine phosphoribosylation and 0.1–6 mM in the case of xanthine phosphoribosylation. Hypoxanthine/guanine concentrations were fixed at 50 μM, and xanthine concentration was fixed at 200 μM. When the concentrations of 6-oxopurines were varied, hypoxanthine and guanine concentrations were varied from 2–50 μM and xanthine concentration was varied from 5–200 μM. PRPP concentration was fixed at 3 mM in these cases. With IMP-activated PfHGXPRT, PRPP concentration was varied from 0.025–1.5 mM in the case of hypoxanthine, guanine, and xanthine phosphoribosylations. The ranges for 6-oxopurine concentrations were the same as those followed for unactivated PfHGXPRT. The concentration of free $MgCl_2$ was maintained at 12 mM for all the assays.

The experimental details for the estimation of kinetic parameters in 10 mM potassium phosphate at pH 7.4 are as follows. PRPP concentration was varied from 0.1–2 mM, 0.1–3 mM and 0.1–5 mM in the case of hypoxanthine, guanine and xanthine phosphoribosylations, respectively, with hypoxanthine/guanine at 50 μM and xanthine at 100 μM. When the 6-oxopurine concentrations were varied, they were maintained between 7.5 and 50 μM and 2.5 and 50 μM, respectively, in the cases of hypoxanthine and guanine. In the case of xanthine, the concentration was maintained between 5 and 100 μM. PRPP concentrations were fixed at 2 mM in all cases. The same range was maintained for both unactivated and IMP-activated states. The concentration of free $MgCl_2$ was maintained at 12 mM for all the assays. v_0 *versus* 6-oxopurine or PRPP concentration was fit to Michaelis–Menten eqn (iv), eqn (v), which represents two K_m values for two different quaternary forms of the enzyme (double hyperbolic equation), and also to Hill's eqn (vi), which represents cooperativity, using Graph Pad Prism, version 5, (Graph Pad Software Inc. San Diego, California).

$$v_0 = (V_{max} \times [S])/(K_m + [S]) \quad \text{(iv)}$$

$$v_0 = V_{max1} \times [S]/(K_{m1} + [S]) + V_{max2} \times [S]/(K_{m2} + [S]) \quad \text{(v)}$$

$$v_0 = V_{max} \times [S]^h/(K' + [S]^h) \quad \text{(vi)}$$

In all the equations, v_0 is the initial velocity at any particular substrate concentration [S]. In the case of unactivated PfHGXPRT, the v_0 values were estimated from the initial steady-state phase of the progress curves after excluding the lag. The duration of the lag phase in each progress curve had been estimated by drawing a tangent from the steady-state phase to the *x*-axis. In Michaelis–Menten eqn (iv), K_m is the Michaelis–Menten constant and V_{max} is the initial velocity at saturating substrate concentration. In eqn (v), K_{m1} and K_{m2} represent the Michaelis–Menten constants for the two different enzyme populations, V_{max1} and V_{max2} are the maximum values of the initial velocities of the two quaternary forms of the enzyme. In eqn (vi), h represents Hill's coefficient and K' is the modified Michaelis–Menten constant, which is a function of several interaction parameters. It is given by $K_m{}^h(a^{h-1}\cdot b^{h-2}\cdot c^{h-3}\cdots z^1)$, wherein a, b, $c\cdots z$ are interaction factors that represent the magnitude by which the K_m value is modified as a result of cooperativity in enzyme behavior. The statistical parameters that were evaluated in order to determine the best fit values were standard errors, 95% confidence intervals and values of regression coefficients (R^2). These experiments have been repeated 2–3 times.

2.6 Computational methods

The enzyme PDB structure [1CJB, *Plasmodium falciparum*],[5] with a resolution of 1.99 Å, was taken from the RCSB Protein Data Bank. Missing residues and atoms were added by the help of GaussView software.[29] The protein was then protonated at neutral pH. Crystal water molecules were deleted from the coordinate file and the protein was solvated by 23 412 SPC/E water molecules[30] in a cubic box of edge length 90.34 Å. Two Na^+ ions were added to neutralize the system. The total energy of the system was then minimized with respect to the coordinates using the steepest descent method. Subsequently, the temperature was increased gradually from 0 K to 300 K over a 50 ps time span in the constant-*NVT* ensemble with a time step of 0.5 fs. This thermalized configuration was utilized to perform long simulation runs in the constant-*NPT* ensemble. A Nośe–Hoover thermostat with a coupling constant of 0.1 ps was employed to maintain the temperature of the system at 300 K, while a Parrinello–Rahman barostat with a coupling constant of 2 ps was utilized to maintain the system at 1 bar pressure. The LINCS algorithm[31] was utilized to keep all the covalent bonds involving hydrogen atoms (C–H, N–H, and O–H) rigid. A time step of 1 fs was used to integrate the equations of motion for all the production runs. However, simulations to obtain the free energy profiles were carried out with a time step of 2 fs constraining all covalent bond lengths (see later). Amber94 force field[32] parameters were used for the protein as well as for the ligands. The interaction potential was cut off at a distance of 12 Å. The Particle Mesh Ewald method was employed to calculate the long range electrostatic interactions. Restrained electrostatic potential (RESP) charges for the ligands were calculated using a RED-vIII server,[33,34] following the protocol described by Bayly *et al.*[35] All simulations were carried out with GROMACS-4.5.5 software.[36–40] Visual Molecular Dynamics (VMD)[41] was used to visualize simulation trajectories. Both VMD and PYMOL[42] software were used to generate the figures.

Given that the barrier for a conformational transition is quite large and is insurmountable with the thermal energy available at ambient conditions within time scales of MD simulations, biased MD simulations were performed on the protein to calculate the free energy profile as a function of the Leu–Lys dihedral angle. These were performed using well-tempered metadynamics (WTM), starting from the loop-opened, ligand-free structure, which itself was obtained from the equilibrium simulation run described earlier. PLUMED-2.0.1 patched with GROMACS-4.5.5 was used to perform the WTM simulations.[43,44] Many biasing techniques exist through which one can calculate the free energy change associated with a rare event of interest. The method of well-tempered metadynamics (WTM)[45] is one of them. Metadynamics[46] and the WTM method have been reviewed well in the literature[47] and have been applied to several problems in biology as well.[48]

3 Results

Earlier studies have shown that purified recombinant PfHGXPRT exhibits weak activity after isolation that increases significantly upon pre-incubation with the product IMP, while GMP and XMP have no effect.[24] We refer to the enzyme that has not been pre-incubated with ligand(s) as the unactivated form and that pre-incubated with ligand(s) as the activated form. The enzyme also exhibits different oligomeric states – dimer and tetramer – whose populations are modulated by PRPP binding and buffer composition.[25] PfHGXPRT is a tetramer in 10 mM potassium phosphate at pH 7.0, and a dimer in 100 mM Tris HCl at pH 7.4 that switches to the catalytically active tetramer upon binding PRPP in presence of $MgCl_2$.[25]

3.1 Catalysis by unactivated PfHGXPRT

PfHGXPRT was purified as described earlier and stored at 253 K (−20 °C) in 10 mM potassium phosphate at pH 7.0, 2 mM DTT and 10% glycerol, at a protein concentration of 200 μM. Xanthine phosphoribosylation assays with unactivated PfHGXPRT were performed under two sets of buffer conditions; 100 mM Tris HCl and 10 mM potassium phosphate, both maintained at pH 7.4. In both buffers, progress curves exhibited a lag phase followed by a steady-state phase accompanied by an increase in product concentration with time (Fig. 2a and Fig. S1a of the ESI†). Under both sets of buffer conditions, at fixed xanthine and PRPP concentrations, the duration of the lag phase decreased with an increase in enzyme concentration. However, even a ten-fold increase (0.2–2 μM) in concentration of PfHGXPRT did not abolish the lag phase. The lag at an enzyme concentration of 2.5 μM (at which PfHGXPRT is a tetramer in phosphate buffer, as shown in Fig. S2 of the ESI†) was also confirmed and the magnitude estimated using a stopped-flow instrument (Fig. S1d and e of the ESI†). The lag phase was also found to decrease with an increase in PRPP concentration (Fig. 2c) when assays were performed at fixed xanthine and PfHGXPRT concentrations. A plot of the duration of the lag phase (τ) *versus* concentration of PfHGXPRT or PRPP showed an inverse relationship in both 100 mM Tris HCl at pH 7.4 and 10 mM potassium phosphate at pH 7.4 (Fig. 2b, d and Fig. S1b of the ESI†), which is characteristic of hysteretic behavior.[49] This resulted in a positive correlation between the value of the rate constant when approaching the steady-state phase from the lag phase, and the concentration of PfHGXPRT or PRPP (Fig. S1c and S3 of the ESI†). The reciprocal of lag duration is the rate constant for the approach from lag to steady-state phase and it represents the process of switching to the active state.[50] However, it should be noted that although the lag reduced, the specific activity values determined from the

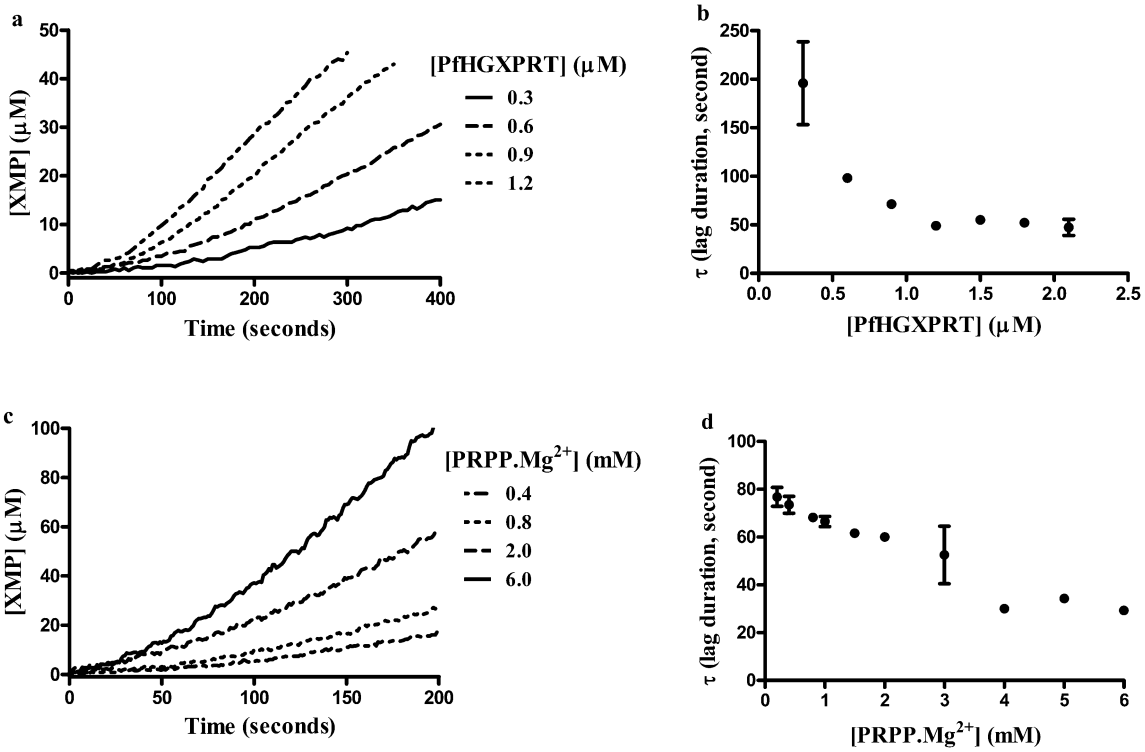

Fig. 2 Hysteretic behavior of unactivated PfHGXPRT in 100 mM Tris HCl at pH 7.4. (a) Representative progress curves of xanthine phosphoribosylation showing a decrease in the duration of the lag phase upon increase in concentration of PfHGXPRT. (b) Inverse relation between lag duration and concentration of PfHGXPRT. (c) Representative progress curves of xanthine phosphoribosylation showing a decrease in the duration of the lag phase upon increase in concentration of PRPP. (d) Inverse relation between lag duration and PRPP concentration. Xanthine concentration was fixed at 200 μM. The duration of the lag phase (τ) was taken as the point of intersection on the x-axis of the line extrapolated from the steady-state phase to $y = 0$. When enzyme concentration was varied, PRPP concentration was fixed at 3 mM. When the concentration of PRPP was varied, PfHGXPRT concentration was fixed at 1 μM. The concentration of free $MgCl_2$ was maintained at 12 mM in all assays. The plots are representative of 3–5 replicate experiments.

steady-state phase of the progress curves remained unchanged with an increase in enzyme concentration.

In order to rule out the possibility that the lag is an artifact of the temperature at which the assays were conducted, xanthine phosphoribosylation by unactivated PfHGXPRT was monitored at different higher temperatures. It was observed that the lag phase persisted even at higher temperatures, but with a reduced duration (Fig. S4 of the ESI†).

A xanthine phosphoribosylation assay with unactivated PfHGXPRT was carried out in D_2O and H_2O to examine the solvent kinetic isotope effect on the duration of the lag phase. The lag durations estimated in D_2O and H_2O were 48.3 seconds and 47.7 seconds, respectively (Section S3 and Fig. S5 of the ESI†), and yielded a rate constant of 120 h^{-1} in both cases.

3.2 Activation of PfHGXPRT

Earlier studies have shown that the initial velocity (and thereby, specific activity) of PfHGXPRT increases when an aliquot of the enzyme pre-incubated with IMP at 273 K for three hours in 10 mM potassium phosphate at pH 7.0 is used to initiate the phosphoribosylation reaction.[24] We extended this study to examine the effect of pre-incubating the enzyme with other substrates or products alone or substrate–product combinations on enzyme activity. The details of the different pre-incubation and assay conditions are provided in the legends to Fig. 3 and Fig. S6 of the ESI.† The enzyme concentration used in all pre-incubations at 273 K was 30 μM, and at this concentration the enzyme is a tetramer in potassium phosphate while tetramer formation in Tris HCl is conditional to the presence of PRPP. Under all conditions, activation of PfHGXPRT was seen when enzyme aliquots pre-incubated with either PRPP·Mg^{2+} or the ligand combinations IMP·PPi·Mg^{2+}/GMP·PPi·Mg^{2+}/hypoxanthine·PPi·Mg^{2+}/guanine·PPi·Mg^{2+} were used for initiation of the phosphoribosylation reaction. The lower level of activation seen with substrate–product combinations of hypoxanthine/guanine·PPi·Mg^{2+} (Fig. 3b and Fig. S6c and d of the ESI†) could be due to the tight nature of association of PfHGXPRT·hypoxanthine (guanine)·PPi dead-end complexes. GMP, XMP, PPi·Mg^{2+} or hypoxanthine alone did not activate the enzyme.

Two important features of PfHGXPRT activation at 273 K, with 30 μM enzyme by all the above ligand(s) were the disappearance of the lag phase and the time dependence for attaining complete activation (Fig. 3a, 4a, Fig. S6a, b and S7a of the ESI†). Even at zero time, the progress curve showed the disappearance of the lag, although the activity was low and comparable to the value shown by the unactivated enzyme (Fig. S7b of the ESI†). It should be noted that 'zero time' represents the earliest time point at which activity could be measured after initiation of pre-incubation. The progress curves recorded at various time durations of PfHGXPRT activation reflect the population that is activated. The time dependence of the increase in specific activity upon pre-incubation at 273 K in potassium phosphate-buffered solution enabled the estimation of rate constants and free energy barriers for the activation process. As the enzyme at 30 μM in potassium phosphate buffer is a tetramer and the process of activation

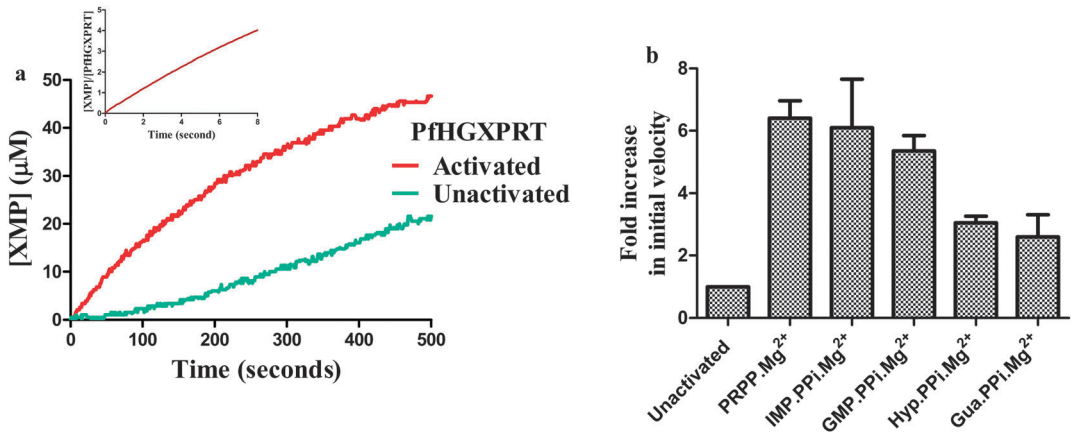

Fig. 3 Activation of PfHGXPRT with different ligand(s). (a) Representative progress curves of xanthine phosphoribosylation by unactivated and activated PfHGXPRT. The inset to this panel shows a progress curve of the phosphoribosylation reaction by activated PfHGXPRT that was obtained using a stopped-flow spectrophotometer. It shows complete absence of the lag phase. For the stopped-flow assay with activated PfHGXPRT, 5 μM activated enzyme in 10 mM potassium phosphate at pH 7.0 was mixed with an assay mix containing 200 μM xanthine, 2 mM PRPP and 26 mM $MgCl_2$ in a 1 : 1 ratio by volume. The total volume of the reaction mix was 126 μl. The total flow rate for mixing was 7 ml s^{-1} with a dead time of 4.3 milliseconds. The duration of the assay was 8 seconds, where each data point was acquired every 1 millisecond, resulting in a total of 8000 data points for the entire trace. (b) Comparison of magnitudes of activation in the presence of different ligand(s) with respect to the unactivated state. For both panels (a and b), the following experimental conditions were maintained. Activation was performed by pre-incubation of 30 μM PfHGXPRT in 10 mM potassium phosphate at pH 7.0 with the different ligand(s), for 3 hours at 273 K. The activated enzyme was directly added to the reaction mixture without prior dilution. Unactivated PfHGXPRT was used as control where, PfHGXPRT at the same concentration was pre-incubated under the same conditions without ligand(s). The ligand(s) are indicated below each bar in the graph. Xanthine phosphoribosylation was monitored in 100 mM Tris HCl at pH 7.4. Xanthine concentration was maintained at 100 μM and PRPP concentration at 1 mM in all the assays. [IMP]/[GMP] carried over to the reaction mix was 0.48 μM. In the case of hypoxanthine and guanine, the concentration carried over was 0.08 μM. The final concentration of PfHGXPRT in the assay mix was 0.2 μM. The plots are representative of 3–5 replicate experiments.

involves the conversion of unactivated tetramers to activated tetramers in the presence of excess PRPP·Mg^{2+}, a first order assumption was applied to estimate the rate constant. The rate constant was estimated by plotting [E′A]/[EA] against the time of incubation. Here, [E′A] represents the concentration of the completely activated PfHGXPRT, which is directly proportional to the initial velocity measured after complete activation of the enzyme. Similarly, [EA] is directly proportional to the initial velocity that is measured at different durations of incubation. 'A' represents the ligand(s) used for activation. The data points were fitted to eqn (vii) for one-phase exponential decay in order to estimate the rate constants that are representative of a first order process, with the dimension of $time^{-1}$.

$$[E'A]/[EA]|_t = (([E'A]/[EA]|_{t=0} - \text{Plateau})e^{-kt}) + \text{Plateau}, \quad \text{(vii)}$$

where k represents the rate constant, t represents duration of pre-incubation in minutes and Plateau is the minimum value of the ratio [E′A]/[EA]. $[E'A]/[EA]|_t$ is the value of the ratio after a particular duration of pre-incubation and $[E'A]/[EA]|_{t=0}$ is the value of the ratio at time 0. One such representative plot that shows first order conversion from [EA] to [E′A] with time is given in Fig. 4b. From these experiments, we found that the rate constant for activation in the presence of PRPP·Mg^{2+} at 273 K is 2.8 h^{-1}. The rate constant can be further converted to the free energy barrier for the activation process using the equation of Eyring and Polanyi:[51,52]

$$k = (k_B T/h)e^{(-\Delta G/RT)}, \quad \text{(viii)}$$

where k is the rate constant for activation obtained from eqn (vii), k_B is the Boltzmann constant, T represents absolute temperature in K, h is Planck's constant, ΔG is the free energy barrier and R is the universal gas constant. The free energy barrier (ΔG) for activation with PRPP·Mg^{2+} was 19.7 kcal mol^{-1}, which is comparable to the value of 19.4 kcal mol^{-1} obtained from the rate constant for the approach from lag to steady-state phase (97 h^{-1}) in the xanthine phosphoribosylation assay in phosphate buffer, monitored using unactivated enzyme in a stopped flow spectrophotometer (Fig. S1d of the ESI†).

The time dependence of activation with PRPP·Mg^{2+} in phosphate buffer was also examined at a higher temperature of 296 K and at protein concentrations of 0.4 and 30 μM. At both enzyme concentrations, the lag disappeared at zero time and complete activation was achieved much faster than at 273 K. While the time taken for complete activation was 3 hours at 30 μM enzyme and 273 K, complete activation was achieved in 15 minutes at 0.4 μM and 296 K (Fig. S8 of the ESI†). Activation at 30 μM and 296 K was fairly rapid and under our experimental conditions, an exact time course could not be measured. As expected, this represents a faster switch to the activated state with increase in temperature.

3.3 Probing the mechanism of IMP binding using the PfHGXPRT mutant W181S/F197W

PfHGXPRT possesses one tryptophan residue, W181, that does not exhibit any change in fluorescence emission properties upon binding IMP. However, F197 in PfHGXPRT interacts with the nucleobase through π–π stacking and hydrophobic interactions[5] and hence, the single tryptophan mutant W181S/F197W was generated to monitor exclusively the report from IMP binding. WT and F197W were included as controls. Upon excitation at 295 nm, the fluorescence spectra at a protein concentration of 5 μM exhibited emission maxima at 340.5 nm for WT and 341.5 nm for F197W and W181S/F197W (Fig. S9a of the ESI†). As expected, the emission intensity of F197W was greater than that of PfHGXPRT due to the presence of two tryptophan residues, whereas in the case of W181S/F197W, although there is one tryptophan as in PfHGXPRT, the emission intensity was lower by approximately seven-fold. Like the wild type enzyme, the mutants in the unactivated state exhibited a lag followed by a steady-state phase (Fig. S9b and c of the ESI†). IMP activation was observed in both F197W and W181S/F197W, and was characterized by an increase in k_{cat} for

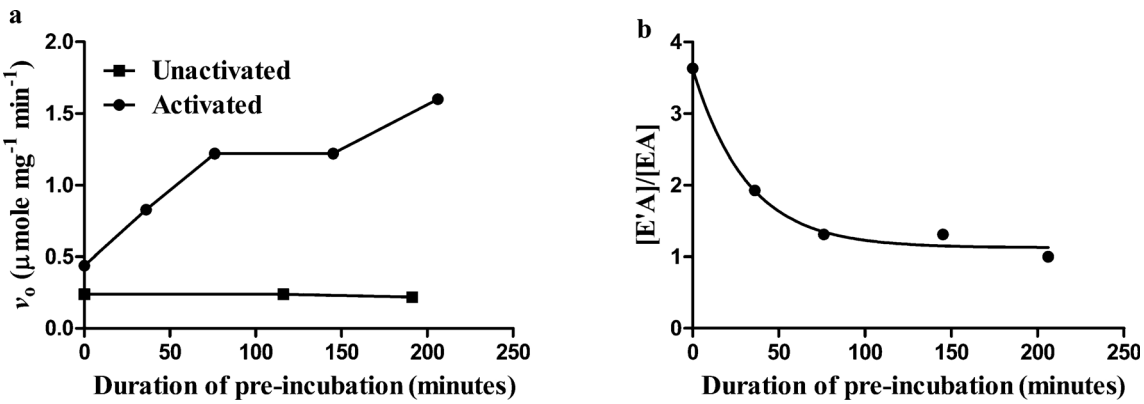

Fig. 4 Effect of duration of pre-incubation on (a) PfHGXPRT activity and (b) concentration of activated species. The initial velocity of the unactivated enzyme remains unchanged with time (panel a). [EA] is directly proportional to the initial velocities measured at different time durations of activation, and [E′A] represents the concentration of completely activated PfHGXPRT that is directly proportional to the initial velocity estimated after complete activation. E represents PfHGXPRT and A indicates the ligand(s) used during activation. Definitions of [EA] and [E′A] are provided in the Section 3.2. As [EA] is gradually converted to [E′A] with time, the ratio of [E′A]/[EA] achieves the value of 1 at the plateau, *i.e.* after complete activation of PfHGXPRT. The plots are representative of 3–5 replicate experiments.

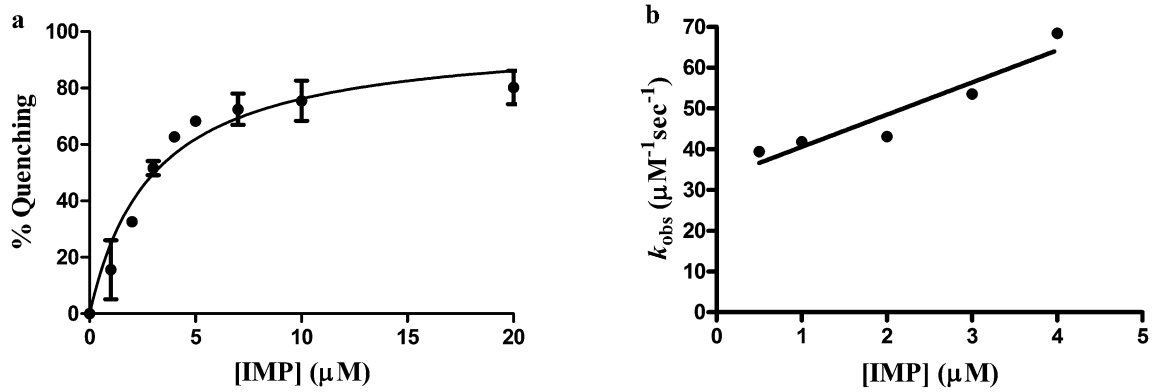

Fig. 5 Mechanism of IMP binding elucidated using the PfHGXPRT mutant W181S/F197W in 10 mM potassium phosphate at pH 7.0. (a) % quenching plotted against IMP concentration using the one-site binding equation (eqn (iii)) to estimate the dissociation constant for the [W181S/F197W·IMP] complex. The excitation wavelength was fixed at 295 nm. IMP concentration was varied from 0.5 μM to 20 μM and the concentration of W181S/F197W was fixed at 5 μM. (b) Positive correlation between k_{obs} and IMP concentration showing the role of both conformational selection and induced fit mechanisms in IMP binding to W181S/F197W. Data points of k_{obs} *versus* [IMP] were fit to a linear equation, which is given as $k_{obs} = k_{on}$[IMP] + k_{off}, in order to estimate the rate constants for IMP binding (k_{on}) and IMP dissociation (k_{off}). The dissociation constant for the W181S/F197W·IMP complex was estimated from the ratio k_{off}/k_{on}. The concentration of W181S/F197W was fixed at 3 μM. IMP concentration was varied from 0.5 μM to 4 μM.

xanthine phosphoribosylation activity and a drop in K_m for PRPP·Mg^{2+} (Table S1 of the ESI†). These mutants were further used for binding studies.

Upon titration of IMP at a fixed concentration of W181S/F197W, the emission intensity was found to decrease (Fig. S10a of the ESI†). The concentration range of IMP used did not exhibit an inner filter effect. From this titration, a K_d value of 3.0 ± 0.6 μM for the W181S/F197W·IMP complex was estimated (Fig. 5a). Values of the rate constants for relaxation to equilibrium upon IMP binding (k_{obs}) measured using a stopped-flow spectrophotometer (Fig. 5b and Fig. S10b of the ESI†) indicated a positive correlation with IMP concentration. Thus, both induced fit and conformational selection mechanisms are likely to be operative in IMP binding. Values of k_{on} and k_{off} were 8×10^6 M^{-1} s^{-1} and 33 ± 4 s^{-1}, respectively. The dissociation constant estimated from the ratio k_{off}/k_{on} was 4 μM and similar to the value obtained from equilibrium measurements. Also, similar values were obtained for the dissociation constant and rate constants of binding and dissociation of IMP in the case of the single mutant F197W (Table S2 of the ESI†). The K_d value for the PfHGXPRT·IMP complex estimated by ITC was 20 μM (Section S4 and Fig. S11 of the ESI†).

3.4 Kinetic characterization of unactivated and activated states of PfHGXPRT

The kinetic parameters of unactivated and IMP-activated PfHGXPRT estimated in 100 mM Tris HCl and in 10 mM potassium phosphate are provided in Table 1. Under unactivated conditions in Tris HCl, the $K_{m(app)}$ value for PRPP was in the mM range and dropped 10–20-fold after activation with IMP, which indicates that IMP activation brings about conformational changes that facilitate PRPP binding. However, the K_m value for the 6-oxopurines remained similar under both conditions. The k_{cat} values, on the other hand, increased by different magnitudes upon IMP activation. In hypoxanthine phosphoribosylation there was no change in k_{cat}, while in guanine and xanthine phosphoribosylation activities, increases in k_{cat} were observed, which were 3- and 5-fold, respectively, over the unactivated versions. On the other hand, in 10 mM potassium phosphate at pH 7.4, activation with IMP resulted primarily in an increase in k_{cat}, which was 3–5-fold in the case of hypoxanthine and xanthine phosphoribosylation and more than 10-fold in the case of guanine phosphoribosylation. Taken together, the kinetic parameters show that the increase in catalytic efficiency (k_{cat}/K_m) upon activation is of greater magnitude when assayed in Tris HCl buffer than in phosphate buffer (Table 1).

The magnitude of the duration of the lag is related to the affinity for PRPP for the inactive state of the enzyme. Use of the relationship[50]

$$\tau = 1/\{k_1 \times ([\text{PRPP}] + K_m)\} \quad \text{(ix)}$$

permits the estimation of the K_m value for PRPP in the lag phase. τ is the duration of the lag and k_1 is k_{cat}/K_m of the enzyme in the lag phase. This yielded a K_m value of 4.8 ± 0.9 mM for PRPP for the xanthine phosphoribosylation reaction with 100 mM Tris HCl at pH 7.4 as the assay buffer. The value of k_1 that corresponds to k_{cat}/K_m of the inactive state of PfHGXPRT with respect to PRPP was 2.8×10^{-6} μM^{-1} s^{-1} (Fig. S12 of the ESI†). The value of k_{cat}/K_{mPRPP} (with respect to PRPP) obtained from the steady-state phase of xanthine phosphoribosylation activity was 1.8×10^{-4} μM^{-1} s^{-1}, which is 60-fold greater than the corresponding value in the inactive state. After complete activation in the presence of IMP, the catalytic efficiency (k_{cat}/K_{mPRPP}) increases further by 167-fold to 3×10^{-2} μM^{-1} s^{-1}. This result clearly shows that PRPP has a weaker affinity for the dimer and the increase in affinity arises from a ligand-induced conformational change associated with tetramerization. This observation is further supported by the high K_m value for PRPP for the PfHGXPRT interface mutant, Y96C, which is impaired in tetramer formation.[25]

Table 1 Kinetic parameters of the unactivated and IMP-activated states of PfHGXPRT[a]

		Unactivated[b]			Activated			
Reaction monitored	Varied substrate	$K_{m(app)}$ (μM)	k_{cat} (s^{-1})	$k_{cat}/K_{m1}\cdot K_{m2}$[c] ($\mu M^{-2}$ s^{-1})	K_m (μM)	k_{cat} (s^{-1})	$k_{cat}/K_{m1}\cdot K_{m2}$[c] ($\mu M^{-2}$ s^{-1})	Ratio[d]
100 mM Tris HCl at pH 7.4								
HPRT	Hypoxanthine	<5	0.20	4.1×10^{-5}	<5	0.30	6.9×10^{-4}	17
	PRPP	972 ± 166	0.20		87 ± 11	0.20		
GPRT	Guanine	<4.8	0.10	1.3×10^{-5}	<5	0.30	6.2×10^{-4}	48
	PRPP	1548 ± 359	0.10		129 ± 23	0.40		
XPRT	Xanthine	78 ± 16	0.20	2.4×10^{-6}	101 ± 27	1.00	1.9×10^{-4}	79
	PRPP	1084 ± 202	0.20		53 ± 10	1.60		
10 mM potassium phosphate at pH 7.4								
HPRT	Hypoxanthine	<5	0.10	1.1×10^{-4}	<7.5	0.3	1.6×10^{-4}	1.4
	PRPP	183 ± 42	0.10		256 ± 66	0.3		
GPRT	Guanine	<2	0.06	7.6×10^{-5}	<2.5	0.4	5.8×10^{-4}	7.6
	PRPP	263 ± 65	0.04		275 ± 69	0.4		
XPRT	Xanthine	45 ± 10	0.30	1.6×10^{-5}	36 ± 11	0.8	3.0×10^{-4}	12.5
	PRPP	277 ± 70	0.20		94 ± 17	1.0		

[a] Enzyme concentrations were fixed at 1 and 0.2 μM for unactivated and IMP-activated PfHGXPRT, respectively. All the kinetic parameters were estimated by fitting the initial velocity data to the Michaelis–Menten equation. K_m values for hypoxanthine and guanine under all conditions have been given as approximations, as activity could not be measured reliably at very low substrate concentrations. Data fitting to the rate equation representing a double hyperbola (eqn (v)) resulted in poor statistical parameters with negative values for one or more kinetic parameters. Fitting of data points to Hill's equation (eqn (vi)) yielded a value of 1 for the Hill's coefficient, which indicates the absence of cooperativity. [b] The v_0 values in the case of unactivated PfHGXPRT were taken from the initial steady-state phase of the progress curves after excluding the lag. Therefore, the kinetic parameters are apparent values. The duration of the lag phase in each progress curve was estimated by drawing a tangent from the steady-state phase to the *x*-axis. The $K_{m(app)}$ values for PRPP being different for unactivated PfHGXPRT in Tris HCl and phosphate-buffered solutions indicates that the initial slopes do report on the different states. [c] K_{m1} and K_{m2} refer to the Michaelis–Menten constants for PRPP·Mg^{2+} and 6-oxopurine, respectively. The values of K_{m2} that have been considered for hypoxanthine and guanine were the minimum concentrations up to which the v_0 values could be measured reliably. [d] Ratio is given by: (catalytic efficiency of activated PfHGXPRT)/(catalytic efficiency of unactivated PfHGXPRT).

3.5 Unbiased MD simulations

The above experimental studies suggest a high energy barrier for the transition from the unactivated to the activated state. A unique feature of HGXPRTs is the presence of a non X-Pro *cis* peptide bond that in some cases is populated only in the ligand-bound state.[2,5,12,13,19,22,23] The interconversion between the *cis* and *trans* conformations is associated with high energy barriers. This observation prompted us to examine the energetics of the *trans* to *cis* isomerisation of the Leu76–Lys77 peptide bond in PfHGXPRT.

Prior to the investigation of the *trans–cis* conformational change of the dipeptide, unbiased molecular dynamics simulations of the ligand-bound and the ligand-free PfHGXPRT were performed. After converting immucillin-HP (in 1CJB) to IMP, the resulting system along with $2Mg^{2+}$–PPi was simulated in water for 120 ns in the *NPT* ensemble to check the stability of the ligands and of the flexible loop. The ligand-free (apo) PfHGXPRT was generated by the removal of the ligand molecules from the active site and simulated for the same time span.

3.5.1 Interactions of PfHGXPRT with IMP·PPi·Mg^{2+}. The MD simulation of ligand-bound PfHGXPRT provides valuable information on the active site region. The active site cavity occupied by the ligand molecules is shown in Fig. 6a. There are three main interaction motifs through which IMP interacts with the protein. The nucleobase is stabilized by (i) π-stacking with Phe197 and hydrogen bonding of N1H with the backbone –CO of Val198, and C6 oxo with ξNH_3^+ of Lys176 (ii) the hydroxyl groups in the sugar ring satisfy the coordination shell of one of the two Mg^{2+} ions present in the pocket. The 5′ phosphate is stabilized by the backbone residues through strong hydrogen bonding interactions with the phosphate oxygens. (iii) Tyr116, present in loop II, stays close to the sugar ring of IMP (Fig. 6b). The last feature is similar to that seen in *Toxoplasma gondii* HGXPRT, wherein the corresponding residue (Tyr118) stabilizes the carbocation that is generated during the catalysis.[53] These interactions maintain the structural features of the otherwise flexible loop by preventing it from opening within the time scale of our simulation. PPi forms a complex with the two Mg^{2+} ions and its O2 and O3 atoms interact with the –NH group of the *cis* conformation of the Leu–Lys dipeptide (Fig. 6c). The puckered ribose structure, earlier reported by Borhani and coworkers,[53] was also observed in the simulation trajectory. The octahedral coordination of one Mg^{2+} ion is satisfied by three water molecules, a carboxylate oxygen of Asp204 and two oxygens from PPi, while the second ion is coordinated to two water molecules, two oxygens each from hydroxyl of ribose and PPi (Fig. 6c). The number of water molecules within 3 Å of any atom of IMP·PPi·$2Mg^{2+}$ is plotted as a function of simulation time in Fig. 6d. 1CJB contains 10 water molecules within the same criterion and thus the result shown in Fig. 6d shows that the crystal waters are intact during the MD trajectory.

3.5.2 Free enzyme. During the simulation of the ligand-free enzyme, a significant movement of loop II was observed between 25–30 ns and it opened spontaneously during this MD trajectory. Its state was quantified through the gate width (defined as the distance between the two Cα atoms of residues Asn206 and

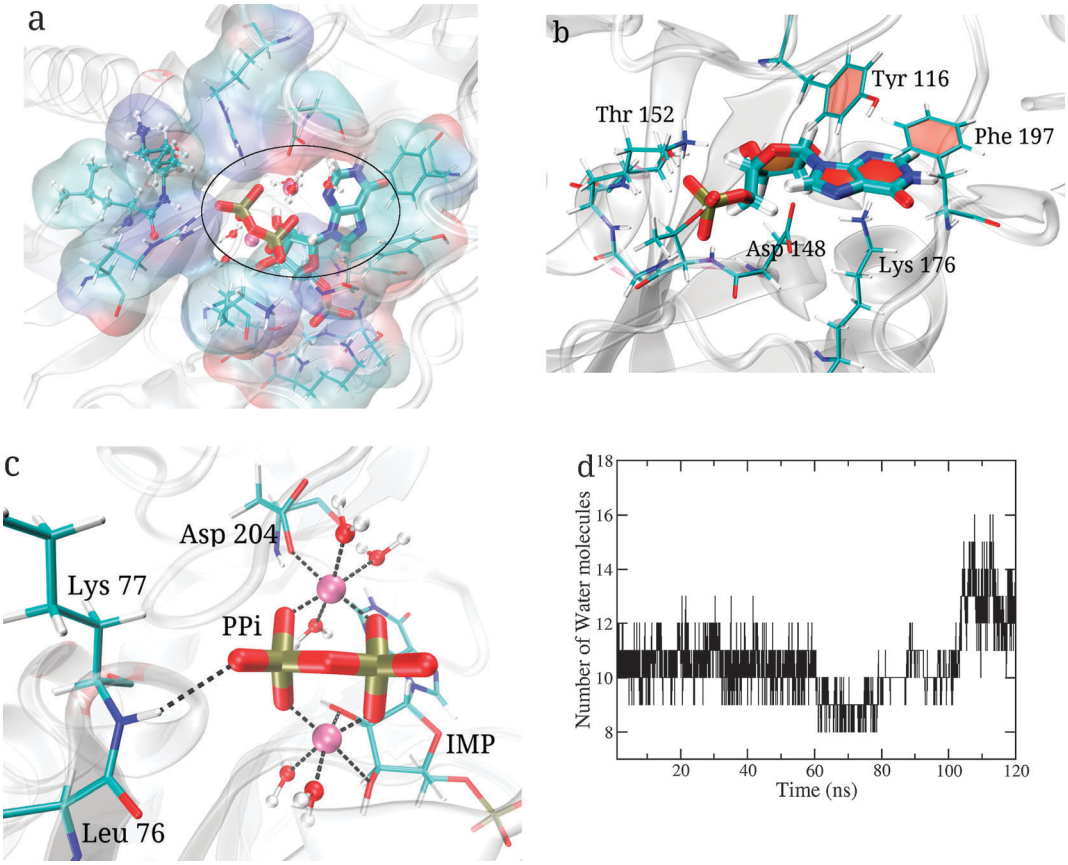

Fig. 6 Ligand interactions and dynamics in PfHGXPRT: (a) active site cavity occupied by ligands; (b) interactions of Tyr116 and Phe197 with IMP; (c) coordination of Mg^{2+}, interaction of PPi with residues; (d) number of water molecules within a 3 Å distance cut-off of any atom of IMP·PPi·Mg^{2+}, plotted as a function of simulation time.

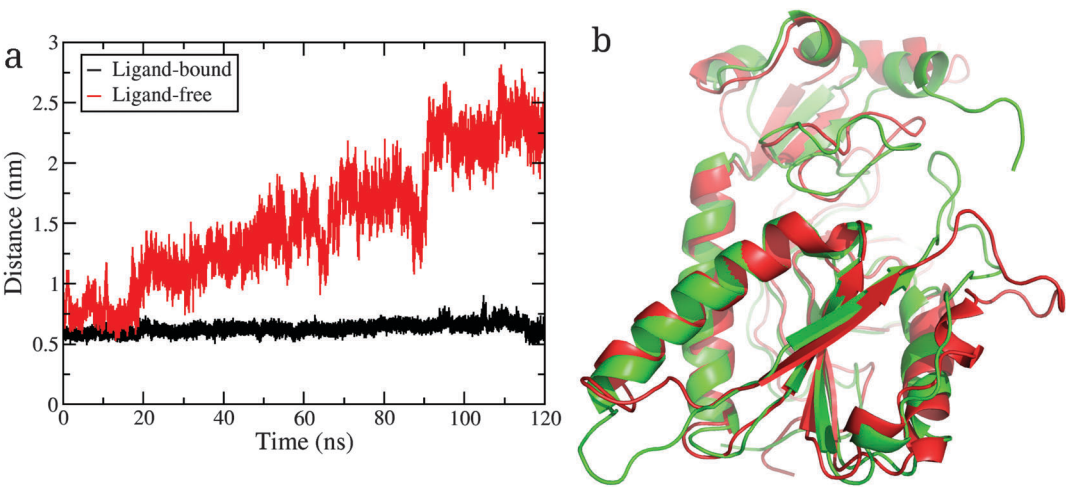

Fig. 7 (a) Gate width (defined as the distance between the two Cα atoms of residues Asn206 and Asn118, located on either end of the gate) *vs.* time during the MD simulations of the ligand-bound (black) and ligand-free (red) enzymes. (b) Overlay of the loop-closed (initial, green) and loop-opened (red) structures obtained during the MD run of the ligand-free enzyme.

Asn118, located on either end of the gate), which attained a maximum value of ~25 Å after 100–110 ns (Fig. 7a and Movie S1 provided in the ESI†). An overlay of the structures with loop II closed and opened is shown in Fig. 7b. We have additionally carried out MD simulations of the ligand-free protein dimer in water for a 100 ns time span in the *NPT* ensemble. Loop II from each of the monomers is seen to open up within a ~20–40 ns time span. Thus the loop opening event reported here appears robust.

The evolution of the Leu–Lys dihedral angle for the ligand-free and the ligand-bound protein (depicted in Fig. S13 of the ESI†) indicate that they are more or less identical, fluctuating around the mean value. Thus as expected, direct, unconstrained MD simulations do not sample slow processes such as the conformational change, within the simulation time scales. Hence, smart methods to sample rare events were employed so as to obtain the free energy difference between the *cis* and the *trans* states of the Leu–Lys dipeptide. As with the initial investigations, the conformational transition of just the Leu–Lys dipeptide was studied in the gas phase and in water using quantum chemical and free energy calculations, respectively. The results of these calculations can be found in Section S5 and Fig. S14 of the ESI.†

3.6 Free energy calculations on PfHGXPRT

The dihedral angle (ω) of the backbone Cα–C–N–Cα of the Leu–Lys dipeptide was chosen to be the collective variable (COLVAR) to calculate the Potential of Mean Force (PMF). The instantaneous change in the collective variable (dihedral angle) with time was captured over the trajectory. An initial bias potential of 0.1 kcal mol^{-1} was applied with a bias factor of 15. Coordinates and parameters of the added Gaussians were saved every 2 ps for further analyses. Four arbitrary configurations from the MD trajectory of the ligand-free enzyme in its loop-opened state were chosen, and WTM runs were initiated from each of them. These are named as FES1, FES2, FES3 and FES4 (Fig. S15 of the ESI†). Each of these runs was carried out for a duration of 200 ns. The ω values ranging from -180° to 180° *via* the *cis* (0°) conformation were explored. The potential of mean force (PMF) along this COLVAR was calculated by using the sum_hills code.[43]

Free energy profiles obtained from the four runs were averaged and are displayed in Fig. 8, while the individual data are provided in Fig. S15 of the ESI.† The *trans* conformation of the dipeptide in the protein is more stable than the *cis* by 12 kcal mol^{-1}, indicating that in the free structure of the protein, the dipeptide is likely to exist in the *trans* conformation. The *cis* to *trans* rotational energy barrier is 13 kcal mol^{-1}, while that in the reverse direction, *i.e.*, from *trans* to *cis*, is around 25 kcal mol^{-1}. This high energy barrier for the conformational change of the dipeptide implies that the conformational switching event is indeed a slow process. PMF calculations of the solvated dipeptide also indicated the stability of the *trans* conformation (Fig. S14b, ESI†). The magnitude of the *cis–trans* free energy difference is larger in the WTM simulations of the full enzyme compared to that for just the dipeptide in water – in the latter, the configuration in which the dipeptide is in the *trans* conformation is additionally stabilized by the interactions with the residues Glu144 and Ile146 (see later).

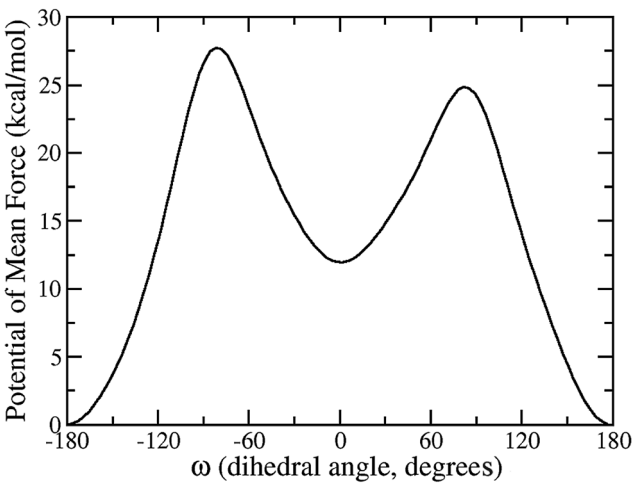

Fig. 8 Free energy profile for the conformational change of the Leu76–Lys77 dipeptide in PfHGXPRT, obtained from well-tempered metadynamics simulations at 300 K.

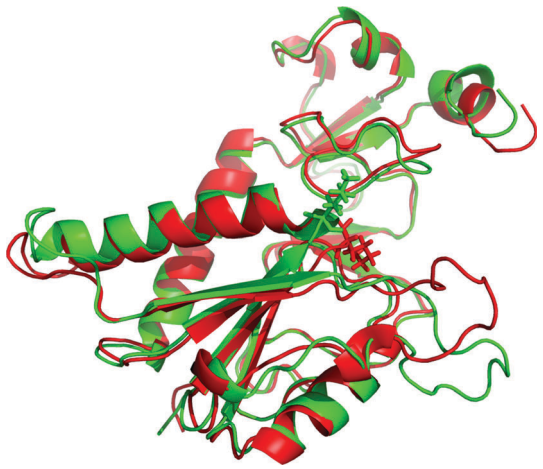

Fig. 9 Overlaid structures of PfHGXPRT with the Leu76–Lys77 present in the *cis* (green) conformation (unbiased MD run), and one obtained from the WTM simulation run where the dipeptide is present in the *trans* (red) conformation.

The ligand-free structure with the dipeptide present in the *cis* conformation obtained from the unbiased simulation was compared with one of the structures extracted from the WTM simulation, wherein the dipeptide is in the *trans* state. An overlay of these two structures is provided in Fig. 9. Significant differences in the orientation of the Lys77 side chain were observed between the two structures. Additional discussions on this comparison are provided in Section S6 of the ESI.† Further, the ligand-free enzyme with the dipeptide present in the *trans* conformation obtained from our WTM simulation was compared with the experimentally determined crystal structure of the human apo enzyme (1Z7G).[13] Reassuringly, the computed ligand-free Pf enzyme has many structural similarities with the human apo enzyme. Thus, the ligand-free Pf enzyme obtained from our simulations can serve as a model structure for further studies. Ligand-free PfHGXPRT with the dipeptide in the *trans* conformation and the loop II in the opened state closely resembles the ligand-free human homolog. Details of the analyses and outcomes are provided in Section S6 and Fig. S18 of the ESI.†

4 Discussion

There are two features associated with PfHGXPRT activity – a lag phase with the unactivated enzyme and activation to an

increased-activity state upon pre-incubation with ligand. The duration of the lag in the progress curves of unactivated PfHGXPRT, in both phosphate- and Tris-buffered solutions, is a function of enzyme and PRPP concentration. This suggests that a ligand-mediated change in equilibrium between dimer and tetramer populations modulates the rate of switch from lag to steady-state phase. However, the limiting lag in enzyme titrations, seen even at concentrations of 1–2 μM in phosphate buffer where the enzyme is a tetramer, suggests the involvement of a (an additional) slower conformational change apart from quaternary dynamics in the process of switch from lag to steady-state phase. Although the reaction progress curves of the unactivated enzyme showed a switch from the lag to the steady-state phase, it was not activated to the fully active state during the time course of the assay. Initiation of the reaction with enzyme pre-incubated with substrates/products abolished the lag in the progress curves and the time dependence of the conversion to the high activity state enabled the estimation of the rate constant and associated free energy barriers for the switch to the activated state. The value of 19–20 kcal mol^{-1} thus obtained corresponds to a conformational change associated with a high energy barrier.[54–57] Human and *T. gondii* HG(X)PRTs exhibit a non-X-Pro (Leu67–Lys68, human numbering) peptide bond isomerization upon PRPP binding; a conformational change needed to create a cavity for accommodating PPi. The rotational energy barrier for Leu76–Lys77 peptide bond rotation in PfHGXPRT estimated from WTM MD simulations is 25.0 kcal mol^{-1} and agrees with the experimental value.

Isomerization of the peptide bond not only creates a cavity for substrate binding but also introduces new inter-subunit interactions. Superposition of the apo, *trans* structure (obtained from the simulation trajectory) (Fig. S19a of the ESI†) and the ligand-bound *cis* structure of PfHGXPRT demonstrates that the isomerization of the Leu76–Lys77 peptide bond in loop I triggers conformational changes in the interface loop (from residues 96–106) at the tetramer (AD) junction (Fig. S19a and S20 of the ESI†) and in the interactions of Lys77. In the *trans* state, the side chain of Lys77 forms a salt bridge with Glu144 within the subunit and, upon isomerization flips across the dimer (AB) interface, with its Nξ establishing a hydrogen bond with the backbone carbonyl of Glu108 of the neighboring subunit (Fig. S19b of the ESI†). It is also interesting to note that the side chain amino group of Lys68 in human HGPRT interacts with side chain carbonyl groups of Asp97[22,58] and Asp119[58] of the neighboring subunit in the *cis* conformation of the Leu67–Lys68 peptide bond.

We propose that the absence of lag subsequent to activation is associated with the formation of a ligand-stabilized *cis* tetramer. During activation in phosphate buffer, the enzyme at the concentration of 30 μM is in the tetrameric form. In the absence of the ligand, the tetramer has the *trans* conformation of the Leu76–Lys77 peptide bond. Dilution of this enzyme to 0.2 μM in the assay mix (Tris/phosphate), yields a progress curve with a lag and a steady-state phase. In the assay mix, the enzyme dissociates to dimers and the hysteretic behavior is a function of [PfHGXPRT] and [PRPP·Mg^{2+}]. During pre-incubation with the ligand in phosphate buffer at 273 K, the enzyme, through a first order process, switches to the *cis*-tetramer state over a period of time. The activated enzyme upon dilution to 0.2 μM in the assay mix does not break up into dimers and hence the absence of lag in the progress curves. The progress curves at various time durations of activation reflect the population that is activated (*trans* tetramer that has switched to the *cis* tetramer in the presence of ligand(s)). Activation of PfHGXPRT at the concentration of 30 μM at 273 K in phosphate buffer has slowed down the process of isomerization and thus permitted its monitoring over time. When PfHGXPRT is activated at the same concentration but at 296 K, the process of isomerization, and therefore also activation, is faster. However, at 0.4 μM PfHGXPRT (at which the oligomeric state could not be determined), the process of activation could involve both oligomerization and isomerization. Hence, it may not be a simple first order process.

In general, the rotational energy barrier about an amide bond is very high ($\sim$15–30 kcal mol^{-1})[59,60] because of its partial double bond character. The close correlation between the values from theory and experiment reveals the robustness of accelerated molecular dynamics simulations for such processes with high energy barriers. The free energy difference between the *cis* and *trans* conformations of the Leu–Lys dipeptide in the ligand-free protein is 12 kcal mol^{-1}. This high magnitude of energy difference is due to the destabilization of the *cis* conformation of the dipeptide in the free enzyme. Based on the structural similarities between the human and the parasite proteins, it can be concluded that the activation process (substrate binding), which is the initial stage of the protein catalytic activity, is associated with the flipping event of the dipeptide from the *trans* (unactivated) to the *cis* (activated) form.

There are three possible mechanisms of isomerization of a peptide bond[61] and these have been discussed in the case of *T. gondii* HGXPRT.[12] A nucleophilic attack on the carbonyl carbon, protonation of the backbone –NH and ligand-mediated conformational twisting about the peptide bond are possible mechanisms of Leu76–Lys77 isomerization in PfHGXPRT. We have evaluated the probable mechanism of isomerization of the peptide bond in PfHGXPRT. Absence of both electron-rich groups in the vicinity of the carbonyl carbon atom and a proton donor in the vicinity of backbone –NH of Lys77 do not support intramolecular nucleophilic attack and protonation-mediated mechanisms for isomerization.[5,23] Further, the similar values for the rate constants for the switch from the lag to the steady-state phase in D_2O and H_2O, obtained from Solvent Kinetic Isotope Effects (SKIE), suggest that protonation of the peptide NH does not catalyze the isomerization. However, under the conditions of the assay (Section S3 and Fig. S5 of the ESI†), we would expect oligomerization and isomerization to be coordinated.

PfHGXPRT activation by isomerization of the Leu76–Lys77 peptide bond and tetramerization is also reflected in the kinetic data. The *trans* dimer of PfHGXPRT (in Tris HCl) has a low affinity for PRPP (with K_m values in the mM range) and upon activation to the *cis* tetramer, the affinity increases, with K_m values dropping to the μM range. In the kinetic measurements

on unactivated PfHGXPRT in phosphate buffer, the lag corresponds to activation to *cis* tetramers and the steady-state phase corresponds to the activated form. The *trans* tetramer of PfHGXPRT (in potassium phosphate) has a higher affinity for PRPP and the increase in k_{cat} upon activation is due to the complete conversion from *trans* tetramers to *cis* tetramers. Under the conditions of multiple turnovers, in the presence of substrates/products, the enzyme does not flip back to the *trans* conformation. In support of this mechanism is the absence of a burst phase (data not shown) in the progress curves of phosphoribosylation using the activated enzyme recorded with a stopped-flow system, a feature unlike the human protein. Further, the rate constants for IMP binding and IMP dissociation were respectively 40-fold and 165-fold greater than k_{cat} of hypoxanthine phosphoribosylation by unactivated PfHGXPRT, which consolidates the fact that catalysis is slower than IMP release. It is interesting to note that the activity of IMP pyrophosphorolysis increased over that of the uninhibited control, when the complex PfHGXPRT·immucillin-GP·PPi·Mg^{2+} was diluted in the reaction mixture.[62] This observation suggests that a conformational feature that is associated with increased activity and induced by the binding of the transition state analog is retained upon inhibitor removal by dilution, highlighting a long timescale for switch to the less active form. IMP binding to PfHGXPRT was found to follow both conformational selection and induced fit mechanisms, as evident from the positive correlation between the overall rate constants for relaxation to equilibrium upon IMP binding (k_{obs}) and ligand concentration. This is also true in the case of PRPP binding, as the rate constants for the approach from lag phase to steady-state phase are dependent on the concentrations of unactivated PfHGXPRT and PRPP.

In *T. gondii* HGXPRT, a thermodynamic framework for the role of isomerization in PRPP binding and release of PPi has been put forth wherein the geometric change serves to avoid low energy kinetic traps. However, the examples where the corresponding dipeptides, Leu46–Arg47 in *E. coli* HPRT,[6] and Ser36–Arg37 in *E. coli* XGPRT,[3] are present in the *cis* conformation in the apo form suggest that in these enzymes the processes of substrate binding and product release occur without any peptide bond interconversion. In some cases, the *cis* conformation of the dipeptide is also retained under the conditions of partial occupancy of the active site.[19,63–66] Fungal HGPRTases are exceptions to all the examples mentioned thus far. *Saccharomyces cerevisiae* HGPRT contains the Gly37–Gly38 peptide bond in the *trans* conformation, the backbone –NH of which hydrogen bonds with the PPi oxygen atoms.[67] The process of isomerization of the dipeptide, which is a slow event, is overcome in *S. cerevisiae* HGPRT by a 13-membered hydrogen-bonded turn in the active site loop I of the enzyme.[67] The role of the dipeptide residues has been extensively investigated by site-directed mutagenesis in different HG(X)PRTs. These mutations resulted in reduced affinity for PRPP, reduced k_{cat} and changes in inter-subunit interactions at the dimer interfaces of the enzymes.[68–72] Diverse phosphoribosyltransferases, such as uracil phosphoribosyltransferase from *Sulfolobus solfataricus* and orotate phosphoribosyltransferase from *Salmonella typhimurium*, also possess a non-X-Pro dipeptide (Leu79–Arg80[73] and Leu73–Gly74,[74] respectively) that switches from the *trans* to the *cis* conformation upon PRPP·Mg^{2+} binding. Examples of enzymes other than PRTases that have non-X-Pro *cis* peptide bonds are human cellular factor XIII and *E. coli* glutamine–PRPP amidotransferase. The former has two non-X-Pro *cis* peptide bonds, which are Arg310–Tyr311 at the active site and Gln425–Phe426 at the dimerization interface,[75] while in the latter, a Pro302–Glu303 dipeptide achieves the *cis* conformation on PRPP binding.[76]

Substrate-induced modulation of oligomeric states has been demonstrated in *Bacillus subtilis* XGPRT.[77] The enzyme exhibited a switch from monomer to dimer in the presence of the substrate PRPP and product XMP. The enzyme without activation showed an initial lag phase followed by a slow linear increase in activity with time, which was attributed to hysteretic behavior of the enzyme in the presence of PRPP. *E. coli* uracil phosphoribosyltransferase also exhibits a dynamic equilibrium between dimers, trimers, pentamers and hexamers. Dimers and trimers had lesser activity whereas the activity shown by the higher oligomeric states was greater. The high activity state could be achieved by GTP, PRPP and guanosine 3′,5′-bis(diphosphate).[78]

The structural dynamics of proteins regulate their function and these conformational switches primarily involve loop movements and global domain movements over hinge regions. Though extremely rare, interconversion of non-X-Pro peptide bonds between *trans* and *cis* conformations plays an important role in the processes of substrate binding and protein oligomerization. Our investigations lead us to conclude that PfHGXPRT presents a unique process of slow activation, modulated by a conformational switch of the non-X-Pro Leu76–Lys77 dipeptide. A complete understanding of the function of PfHGXPRT could be of added value to the ongoing efforts[22,23,58,79,80] in the development of inhibitors to the enzyme.

Acknowledgements

T. K. and S. B. acknowledge the Department of Science and Technology for support. S. B. thanks Sheikh Saqr Laboratory, ICMS for a fellowship. V. S. P. R acknowledges DBT for a postdoctoral fellowship, L. K. N acknowledges the Council of Scientific and Industrial Research for a Junior Research Fellowship, H. B. acknowledges the Department of Science and Technology and the Department of Biotechnology for funding. The DNA sequencing facility at MBGU, JNCASR is acknowledged for providing DNA sequence of the mutants.

References

1 J. C. Eads, G. Scapin, Y. Xu, C. Grubmeyer and J. C. Sacchettini, *Cell*, 1994, **78**, 325–334.
2 M. A. Schumacher, D. Carter, D. S. Roos, B. Ullman and R. G. Brennan, *Nat. Struct. Biol.*, 1996, **3**, 881–887.
3 S. Vos, R. J. Parry, M. R. Burns, J. de Jersey and J. L. Martin, *J. Mol. Biol.*, 1998, **282**, 875–889.

4 P. J. Focia, S. P. Craig, R. Nieves-Alicea, R. J. Fletterick and A. E. Eakin, *Biochemistry*, 1998, **37**, 15066–15075.
5 W. Shi, C. M. Li, P. C. Tyler, R. H. Furneaux, S. M. Cahill, M. E. Girvin, C. Grubmeyer, V. L. Schramm and S. C. Almo, *Biochemistry*, 1999, **38**, 9872–9880.
6 L. W. Guddat, S. Vos, J. L. Martin, D. T. Keough and J. de Jersey, *Protein Sci.*, 2002, **11**, 1626–1638.
7 R. Schmidt, H. Wiegand and U. Reichert, *Eur. J. Biochem.*, 1979, **93**, 355–361.
8 Y. Xu and C. Grubmeyer, *Biochemistry*, 1998, **37**, 4114–4124.
9 N. R. Munagala and C. C. Wang, *Biochemistry*, 1998, **37**, 16612–16619.
10 N. Munagala, V. J. Basus and C. C. Wang, *Biochemistry*, 2001, **40**, 4303–4311.
11 B. Ullman, N. Cyr, K. Choi and A. Jardim, *Int. J. Biochem. Cell Biol.*, 2010, **42**, 253–262.
12 A. Héroux, E. L. White, L. J. Ross, R. L. Davis and D. W. Borhani, *Biochemistry*, 1999, **38**, 14495–14506.
13 D. T. Keough, I. M. Brereton, J. De Jersey and L. W. Guddat, *J. Mol. Biol.*, 2005, **351**, 170–181.
14 A. Giacomello and C. Salerno, *J. Biol. Chem.*, 1978, **253**, 6038–6044.
15 Y. Xu, J. Eads, J. C. Sacchettini and C. Grubmeyer, *Biochemistry*, 1997, **36**, 3700–3712.
16 L. Yuan, S. P. Craig III, J. H. McKerrow and C. C. Wang, *Biochemistry*, 1992, **31**, 806–810.
17 S. A. Queen, D. Vander Jagt and P. Reyes, *Mol. Biochem. Parasitol.*, 1988, **30**, 123–133.
18 R. G. Donald, D. Carter, B. Ullman and D. S. Roos, *J. Biol. Chem.*, 1996, **271**, 14010–14019.
19 A. Héroux, E. L. White, L. J. Ross and D. W. Borhani, *Biochemistry*, 1999, **38**, 14485–14494.
20 J. W. Pitera, N. R. Munagala, C. C. Wang and P. A. Kollman, *Biochemistry*, 1999, **38**, 10298–10306.
21 A. Thomas and M. J. Field, *J. Am. Chem. Soc.*, 2006, **128**, 10096–10102.
22 W. Shi, C. M. Li, P. C. Tyler, R. H. Furneaux, C. Grubmeyer, V. L. Schramm and S. C. Almo, *Nat. Struct. Biol.*, 1999, **6**, 588–593.
23 K. Z. Hazleton, M.-C. Ho, M. B. Cassera, K. Clinch, D. R. Crump, I. Rosario Jr, E. F. Merino, S. C. Almo, P. C. Tyler and V. L. Schramm, *Chem. Biol.*, 2012, **19**, 721–730.
24 J. Raman, C. S. Ashok, S. IN Subbayya, R. P. Anand, S. T. Selvi and H. Balaram, *FEBS J.*, 2005, **272**, 1900–1911.
25 I. Subbayya and H. Balaram, *FEBS Lett.*, 2002, **521**, 72–76.
26 G. Sarkar and S. S. Sommer, *BioTechniques*, 1990, **8**, 404–407.
27 C. Salerno and A. Giacomello, *J. Biol. Chem.*, 1981, **256**, 3671–3673.
28 E. C. Hulme and M. A. Trevethick, *Br. J. Pharmacol.*, 2010, **161**, 1219–1237.
29 R. Dennington, T. Keith and J. Millam, Semichem Inc., Shawnee Mission KS, 2009.
30 H. J. C. Berendsen, J. R. Grigera and T. P. Straatsma, *J. Phys. Chem.*, 1987, **91**, 6269–6271.
31 B. Hess, H. Bekker, H. J. Berendsen and J. G. Fraaije, *et al.*, *J. Comput. Chem.*, 1997, **18**, 1463–1472.
32 W. D. Cornell, P. Cieplak, C. I. Bayly, I. R. Gould, K. M. Merz, D. M. Ferguson, D. C. Spellmeyer, T. Fox, J. W. Caldwell and P. A. Kollman, *J. Am. Chem. Soc.*, 1996, **118**, 2309.
33 E. Vanquelef, S. Simon, G. Marquant, E. Garcia, G. Klimerak, J. C. Delepine, P. Cieplak and F.-Y. Dupradeau, *Nucleic Acids Res.*, 2011, **39**, W511–W517.
34 F.-Y. Dupradeau, A. Pigache, T. Zaffran, C. Savineau, R. Lelong, N. Grivel, D. Lelong, W. Rosanski and P. Cieplak, *Phys. Chem. Chem. Phys.*, 2010, **12**, 7821–7839.
35 C. I. Bayly, P. Cieplak, W. Cornell and P. A. Kollman, *J. Phys. Chem.*, 1993, **97**, 10269–10280.
36 H. J. Berendsen, D. van der Spoel and R. van Drunen, *Comput. Phys. Commun.*, 1995, **91**, 43–56.
37 D. Van Der Spoel, E. Lindahl, B. Hess, G. Groenhof, A. E. Mark and H. J. Berendsen, *J. Comput. Chem.*, 2005, **26**, 1701–1718.
38 B. Hess, C. Kutzner, D. Van Der Spoel and E. Lindahl, *J. Chem. Theory Comput.*, 2008, **4**, 435–447.
39 S. Pronk, S. Páll, R. Schulz, P. Larsson, P. Bjelkmar, R. Apostolov, M. R. Shirts, J. C. Smith, P. M. Kasson and D. van der Spoel, *et al.*, *Bioinformatics*, 2013, btt055.
40 E. Lindahl, B. Hess and D. Van Der Spoel, *J. Mol. Model.*, 2001, **7**, 306–317.
41 W. Humphrey, A. Dalke and K. Schulten, *J. Mol. Graphics*, 1996, **14**, 33–38.
42 L. Schrödinger, *Py-MOL*, *The PyMOL Molecular Graphics System*, Version, 2010, vol. 1.
43 M. Bonomi, D. Branduardi, G. Bussi, C. Camilloni, D. Provasi, P. Raiteri, D. Donadio, F. Marinelli, F. Pietrucci and R. A. Broglia, *et al.*, *Comput. Phys. Commun.*, 2009, **180**, 1961–1972.
44 G. A. Tribello, M. Bonomi, D. Branduardi, C. Camilloni and G. Bussi, *Comput. Phys. Commun.*, 2014, **185**, 604–613.
45 A. Barducci, G. Bussi and M. Parrinello, *Phys. Rev. Lett.*, 2008, **100**, 020603.
46 A. Laio and F. L. Gervasio, *Rep. Prog. Phys.*, 2008, **71**, 126601.
47 A. Barducci, M. Bonomi and M. Parrinello, *Biophys. J.*, 2010, **98**, L44–L46.
48 J. Xia and R. M. Levy, *J. Phys. Chem. B*, 2014, **118**, 4535–4545.
49 C. Frieden, *Annu. Rev. Biochem.*, 1979, **48**, 471–489.
50 R. G. Silva and V. L. Schramm, *Biochemistry*, 2011, **50**, 9158–9166.
51 H. Eyring, *J. Chem. Phys.*, 1935, **3**, 107–115.
52 K. J. Laidler and M. C. King, *J. Phys. Chem.*, 1983, **87**, 2657–2664.
53 A. Héroux, E. White, L. J. Ross, A. P. Kuzin and D. W. Borhani, *Structure*, 2000, **8**, 1309–1318.
54 P. Craveur, A. P. Joseph, P. Poulain, A. G. de Brevern and J. Rebehmed, *Amino Acids*, 2013, **45**, 279–289.
55 E. A. Basso, P. R. Oliveira, F. Wiectzycoski, R. M. Pontes and B. C. Fiorin, *J. Mol. Struct.*, 2005, **753**, 139–146.
56 A. P. Joseph, N. Srinivasan and A. G. De Brevern, *Amino Acids*, 2012, **43**, 1369–1381.
57 T. Shen, D. Hamelberg and J. A. McCammon, *Phys. Rev. E: Stat., Nonlinear, Soft Matter Phys.*, 2006, **73**, 041908.
58 D. T. Keough, D. Hockova, Z. Janeba, T.-H. Wang, L. Naesens, M. D. Edstein, M. Chavchich and L. W. Guddat, *J. Med. Chem.*, 2015, **58**, 827–846.

59 Y. A. Mantz, D. Branduardi, G. Bussi and M. Parrinello, *J. Phys. Chem. B*, 2009, **113**, 12521.
60 C. Melis, G. Bussi, S. C. R. Lummis and C. Molteni, *J. Phys. Chem. B*, 2009, **113**, 12148.
61 S. T. Park, R. A. Aldape, O. Futer, M. T. DeCenzo and D. J. Livingston, *J. Biol. Chem.*, 1992, **267**, 3316–3324.
62 C. M. Li, P. C. Tyler, R. H. Furneaux, G. Kicska, Y. Xu, C. Grubmeyer, M. E. Girvin and V. L. Schramm, *Nat. Struct. Biol.*, 1999, **6**, 582–587.
63 W. Shi, N. R. Munagala, C. C. Wang, C. M. Li, P. C. Tyler, R. H. Furneaux, C. Grubmeyer, V. L. Schramm and S. C. Almo, *Biochemistry*, 2000, **39**, 6781–6790.
64 Q. Chen, Y. Liang, X. Su, X. Gu, X. Zheng and M. Luo, *J. Mol. Biol.*, 2005, **348**, 1199–1210.
65 M. Kanagawa, S. Baba, A. Ebihara, A. Shinkai, K. Hirotsu, R. Mega, K. Kim, S. Kuramitsu, G.-I. Sampei and G. Kawai, *Acta Crystallogr., Sect. F: Struct. Biol. Cryst. Commun.*, 2010, **66**, 893–898.
66 P. S. Monzani, S. Trapani, O. H. Thiemann and G. Oliva, *BMC Struct. Biol.*, 2007, **7**, 59.
67 L. Moynié, M.-F. Giraud, A. Breton, F. Boissier, B. Daignan-Fornier and A. Dautant, *Protein Sci.*, 2012, **21**, 1185–1196.
68 J. P. Page, N. R. Munagala and C. C. Wang, *Eur. J. Biochem.*, 1999, **259**, 565–571.
69 N. R. Munagala, M. S. Chin and C. C. Wang, *Biochemistry*, 1998, **37**, 4045–4051.
70 B. Canyuk, F. J. Medrano, M. A. Wenck, P. J. Focia, A. E. Eakin and S. P. Craig III, *J. Mol. Biol.*, 2004, **335**, 905–921.
71 A. C. Butterworth, F. J. Medrano, A. E. Eakin and S. P. Craig III, *Biochim. Biophys. Acta, Proteins Proteomics*, 2004, **1699**, 87–94.
72 G. K. Balendiran, J. Molina, Y. Xu, J. Torres-Martinez, R. Stevens, P. J. Focia, A. E. Eakin, J. C. Sacchettini and S. P. Craig, *Protein Sci.*, 1999, **8**, 1023–1031.
73 S. Christoffersen, A. Kadziola, E. Johansson, M. Rasmussen, M. Willemöes and K. F. Jensen, *J. Mol. Biol.*, 2009, **393**, 464–477.
74 L. González-Segura, J. F. Witte, R. W. McClard and T. D. Hurley, *Biochemistry*, 2007, **46**, 14075–14086.
75 M. S. Weiss, H. J. Metzner and R. Hilgenfeld, *FEBS Lett.*, 1998, **423**, 291–296.
76 C. R. Muchmore, J. M. Krahn, J. L. Smith, J. H. Kim and H. Zalkin, *Protein Sci.*, 1998, **7**, 39–51.
77 S. Arent, A. Kadziola, S. Larsen, J. Neuhard and K. F. Jensen, *Biochemistry*, 2006, **45**, 6615–6627.
78 K. F. Jensen and B. Mygind, *Eur. J. Biochem.*, 1996, **240**, 637–645.
79 K. Clinch, D. R. Crump, G. B. Evans, K. Z. Hazleton, J. M. Mason, V. L. Schramm and P. C. Tyler, *Bioorg. Med. Chem.*, 2013, **21**, 5629–5646.
80 O. Baszczyński, D. Hocková, Z. Janeba, A. Holý, P. Jansa, M. Dračínský, D. T. Keough and L. W. Guddat, *Eur. J. Med. Chem.*, 2013, **67**, 81–89.

